Central European Journal of Energetic Materials, **2013**, *10*(3), 359-369
ISSN 1733-7178

Thermally Induced Damage in Hexanitrohexaazaisowurtzitane

Qiang TIAN[1], Guanyun YAN[1], Guangai SUN[1], Chaoqiang HUANG[1], Lei XIE[1], Bo CHEN[1], Ming HUANG[2], Hongzhen LI[2], Yi LIU[3] and Jie WANG[3]

[1]*Key Laboratory for Neutron Physics and Institute of Nuclear Physics and Chemistry, China Academy of Engineering Physics, Mianyang 621900, China*
[2]*Institute of Chemical Materials, China Academy of Engineering Physics, Mianyang 621900, China*
[3]*Institute of Shanghai Apply Physics, Chinese Academy of Science, Shanghai 201800, China*
E-mail: tqsuperego@163.com

Abstract: The evolution of the microstructure of hexanitrohexaazaisowurtzitane (CL-20) after a thermal stimulus plays a key role in the performance of CL-20. In the current work, microstructural variations of CL-20 caused by thermal treatment were investigated by X-ray diffraction, in situ variable-temperature optical microscopy, atom force microscopy, and small-angle X-ray scattering. A wave-like process, an abrupt volume expansion, movement, and fragmentation of CL-20 particles during phase transition were observed. After the phase transition (160 °C) the CL-20 sample acquired a very rough surface with numerous dimple depressions, and during the thermal decomposition stage (200 °C) a large number of voids were produced in both the bulk and the surface of the CL-20.

Keywords: CL-20, SAXS, AFM, thermal effects, voids

Introduction

When energetic materials are subjected to unintentional heating, such as fire, earthquakes, fall, sudden climate change, and combat operations in battlefields,

the thermal effects could result in voids, cracking, phase transitions, thermal expansion, and gaseous decomposition. All of these modifications alter the physical and chemical properties, as well as the equation of state, of the energetic materials. The resulting damaged energetic materials will become more sensitive to shock or impact initiation [1]. Therefore, characterizing and understanding the thermal effects on energetic materials is important.

Hexanitrohexaazaisowurtzitane (CL-20), considered to be the most powerful, high-energy molecular explosive today, has a cage structure and a chemical formula of $C_6H_6N_{12}O_{12}$ [2]. Compared with cyclotetramethylenetetranitramine (HMX), CL-20 is envisaged to deliver 20% higher performance. However, the phase transition of CL-20 from ε to γ occurs readily at 140-170 °C, and its thermal stability is lower than that of HMX [5]. Therefore, it is necessary and significant to study the thermal damage caused in CL-20. The thermal decomposition characteristics and by-products have been studied using differential scanning calorimetry and pyrolysis gas chromatography–mass spectrometry [3, 4]. However, only a few studies on the defects in damaged CL-20 after thermal treatment are available to date.

Many techniques have been employed to characterize the defects in energetic materials [6]. Among these methods, the small-angle scattering (SAS) technique is a very powerful tool for investigating nanoscale defects in explosives. A series of experiments on HMX and triaminotrinitrobenzene-based polymer-bonded explosives that had suffered thermal damage has been carried out using small-angle X-ray scattering (SAXS) and small-angle neutron scattering at Los Alamos and Lawrence Livermore National Laboratories [7-9]. Mang *et al*. [7] revealed the development of large pores, cracks, and morphological changes in HMX, associated with the β–δ phase transition at approximately 180 °C. The CL-20 microstructural changes caused by thermal treatment has never been studied by SAS until now. In the present work, the evolution of the CL-20 microstructure during thermal treatment was characterized by in situ variable-temperature, optical microscopy (OM), X-ray diffraction (XRD), and atom force microscopy (AFM). SAXS was then employed to trace variations in the total interfacial surface area, void sizes, distribution, and volume ratios of CL-20 powders.

Materials and Methods

Insensitive CL-20 crystalline powders, provided by the Institute of Chemical Materials, China Academy of Engineering Physics, were grown from mixed solvents by controlling the evaporation rate. The average size of the as-prepared

CL-20 was approximately 50 μm. In situ variable-temperature OM images were taken using an Olympus BX51 optical microscope at a heating rate of 2 °C/min. The surface morphology of the CL-20 samples was investigated using AFM (SPA300HV, Seiko Instrument Inc., Chiba, Japan) under ambient conditions. The CL-20 crystalline powders were dispersed on glass slides before AFM measurements and dynamic force mode images were taken with an ultra-sharp Si cantilever with a tip curvature of 50 nm. XRD measurements were performed on a PANalytical X-Pert PRO diffractometer using Cu K_α radiation. Prior to SAXS, AFM, and XRD measurements, batches of the same CL-20 powder were heated in an ageing chamber at 150, 160, and 170 °C for 1 h, as well as at 200 °C for 1, 3, and 5 h. The samples were then allowed to cool naturally to room temperature. The SAXS measurements were conducted at the SAXS station (BL16B1) in Shanghai Synchrotron Radiation Facility (SSRF), China. SSRF, which comprises a 3.5 GeV electron storage ring, a full energy booster, and a 150 MeV linac, is a third-generation light source. The radiation from the storage ring is monochromatized using a Si(111) double crystal monochromator. The incident beam is restricted by a set of *x*–*y* slits, and the focused spot size is 0.5×0.4 mm^2. Two-dimensional (2D) scattering patterns were recorded using an image-intensified, charge-coupled device detector. The X-ray wavelength was 0.154 nm, and the distance between the detector and the sample was 5.1 m. Conversion of the 2D data to one-dimensional curves and data fitting were performed using the MySAS package [10]. The relative scattering intensities were calculated by

$$I=\frac{I_1}{K_1}-\frac{I_2}{K_2}$$

where I_1 and I_2 are the measured intensities of the sample and empty specimen holder, respectively; K_1 and K_2 are the corresponding back monitor counts.

Results and Discussion

The in situ variable-temperature optical micrographs of the CL-20 samples are shown in Figure 1. No changes are observed up to 165 °C. As the temperature was increased up to 170 °C, a wave-like process in some particles, with a very fast transition, was observed. Chukanov *et al*. [5, 11] regarded this wave-like process as a phase-transition wave. Further abrupt volume expansion and fragmentation of some particles was observed, and some crystallites suddenly 'jumped' in and out of the field of view (Figure 1). The XRD patterns of the CL-20 samples after heating

at 150, 160, 170, and 200 °C for 1 h are shown in Figure 2. Obvious changes in the patterns were observed when the temperature rose from 150 to 160 °C. By comparison with the XRD patterns in the literature [12, 13], the conclusion can be drawn that the ε phase remained up to 150 °C and then transformed into the γ phase at 160 °C. No weight loss accompanied this thermal phase transition. The densities of ε- and γ-CL-20 are 2.04 and 1.92 g/cm^3, respectively. Hence, the CL-20 volume increases by 6% after phase transition from ε to γ, which could lead to stress cracking, as shown in the regions of the white circles in Figures 1(a) and (b). The AFM image of the CL-20 sample after heating at 150 °C for 1 hour (Figure 3(a)) exhibited a flat surface having voids with sizes ranging from 20 to 300 nm. After heating at 160 °C for 1 h the sample had a very rough surface, with numerous dimple depressions through the image, (Figure 3(b)). A number of voids with sizes ranging from a few nanometers to a few hundred nanometers existed at the surface of the CL-20 sample after heating at 200 °C for 1 h (Figure 3(c)). A 50% mass loss was observed after the sample had been heated at 200 °C for 5 h. Therefore, voids were also produced in the bulk.

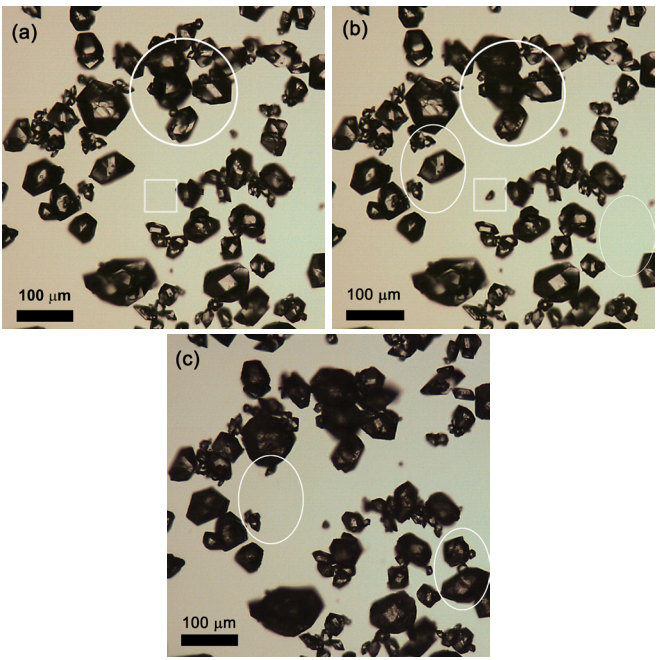

Figure 1. In situ variable-temperature OM images of the CL-20 samples heated to (a) 165, (b) 170, and (c) 200 °C at a heating rate of 2 °C/min. The white circles, ovals, and squares in the figure represent noticeable changes in the samples.

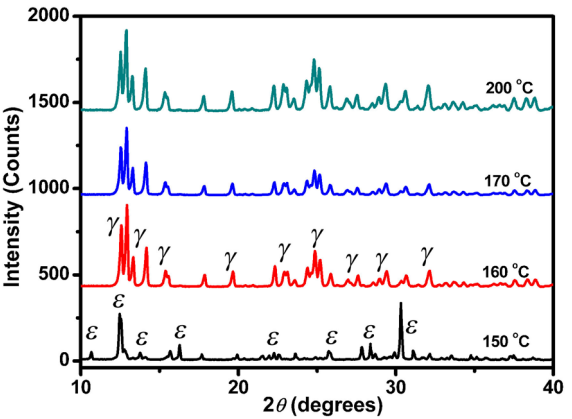

Figure 2. XRD patterns of the CL-20 samples after heating at 150, 160, 170, and 200 °C for 1 h.

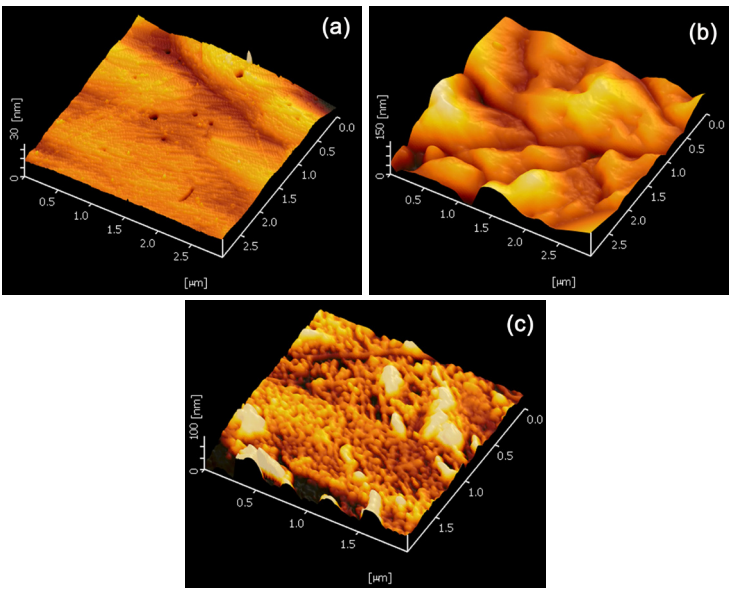

Figure 3. AFM images of the CL-20 samples after heating at (a) 150, (b) 160, and (c) 200 °C for 1 h. (a) Scan size is 3×3 μm^2, and the *z* scale is 30 nm. (b) Scan size is 3×3 μm^2, and the *z* scale is 150 nm. (c) Scan size is 2×2 μm^2, and the *z* scale is 100 nm.

The 2D SAXS images of the CL-20 samples after heating at 150 and 160 °C for 1 h are shown in Figure 4. The logI–logq curves converted from Figure 4

are shown in Figure 5. Log-normal distribution has already been proven to be a reasonable model for energetic materials [9, 14]. In the present paper, we attempt to explain the SAXS data by modelling the system in terms of a polydisperse system of spherical voids and log-normal distribution, *i.e*.

$$I(q)=(\frac{4\pi}{3})^2 N_0 \Delta\rho^2 \int_0^\infty f(R)R^6F^2(qR)dR \quad (1)$$

$$f(R)=\frac{1}{\sigma R\sqrt{2\pi}}\exp[-\frac{1}{2\sigma^2}(\ln(R)-\mu)^2] \quad (2)$$

$$F(qR)=\frac{\sin(qR)-qR\cos(qR)}{(qR)^3} \quad (3)$$

$$S_v=4\pi\left\langle R^2\right\rangle N_0=3\phi\exp(-\mu-\frac{5}{2}\sigma^2) \quad (4)$$

where N_0 is the total number of voids per unit volume; $\Delta\rho$ is the difference in scattering length density between the CL-20 and the voids, and $\mu = \ln(R_{med})$ (R_{med} is the median radius); f(R) is the log-normal size distribution; F(qR) is the scattering amplitude of the void; ϕ is the fitted volume ratio, and S_v is the total interfacial surface area per unit sample volume. The fitted results are listed in Table 1. The S_v and ϕ of the sample after heating at 150 °C for 1 h are normalized as one. Here, we consider the sample heated at 150 °C as the baseline data for comparison with the other thermally treated samples because the as-prepared CL-20 is very stable below 150 °C. There exists a small deviation of the experimental data points from the best fit at $q = 0.2$ nm^{-1} in Figure 5, which may be attributed to the presence of a small quantity of nonspherical defects in the samples. When the temperature was increased to 170 °C, S_v and ϕ increased by 5.4 and 5.2-fold, respectively. The median void radius in CL-20 increased from 79 to 84 nm after the phase transition. The scattering intensity of γ-CL-20 increased significantly with increasing heating time at 200 °C (Figure 6(a)), which illustrates that a large number of voids were produced during the thermal decomposition process, as shown in Figure 3(c). Compared with the scattering curve of the sample heated at 150 °C, the relative intensity of the sample heated at 200 °C became strong in the high q region (>0.1 nm^{-1}) because a second population of smaller voids, with sizes of approximately 10 nm, was developed. Hence, bimodal log-normal size distributions were adopted to fit the I–q curve. The solid lines are the fitted results, and are in good agreement with the measured data (Figure 6(a)). Figures 6(b) and (c) show the f(R) of the large and small

voids, respectively, obtained by model fitting. The distributions shift towards larger median void sizes with increasing holding time at 200 °C. By contrast to the sample heated at 150 °C for 1 h, the S_v and ϕ values of the sample heated at 200 °C for 5 h increased by factors of about 1.4×10^3 and 2.0×10^3 respectively for large voids with a median size of 120 nm, as well as by factors of about 4.8×10^3 and 8.5×10^2 respectively for small voids with a median size of 12 nm, during the thermal decomposition. The fitted results are reported in Table 2.

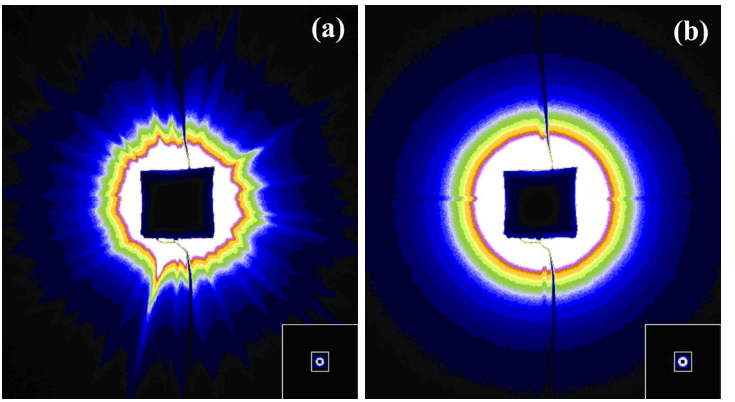

Figure 4. SAXS images of the CL-20 samples after heating at (a) 150 and (b) 160 °C for 1 h.

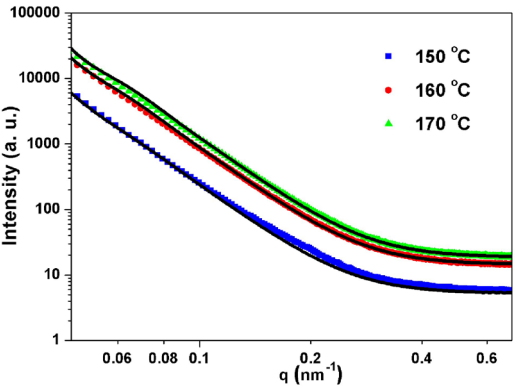

Figure 5. SAXS data of the CL-20 samples after heating at 150, 160, and 170 °C for 1 h. Solid lines represent the fitted results.

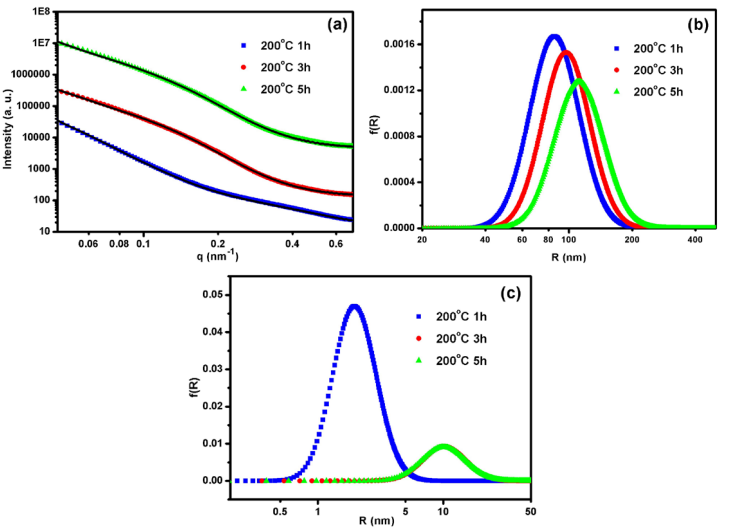

Figure 6. (a) SAXS data and log-normal distribution of (b) large voids and (c) small voids of the CL-20 samples after heating at 200 °C for 1, 3, and 5 h. The solid lines in (a) are the fitted results of bimodal log-normal size distributions.

Table 1. Fitted results of CL-20 before and after the phase transition

Thermal conditions	Surface area	Volume ratio	Median radius (nm)
150 °C 1 h	1	1	79
160 °C 1 h	3.8	3.8	84
170 °C 1 h	5.4	5.2	84

Table 2. Fitted results of CL-20 during thermal decomposition at 200 °C

Thermal conditions	Voids	Surface area	Volume ratio	Median radius (nm)
200 °C 1 h	large voids	22	8	92
200 °C 3 h		45	56	104
200 °C 5 h		1.4×10^3	2.0×10^3	120
200 °C 1 h	small voids	60	2	2
200 °C 3 h		1.4×10^2	24	12
200 °C 5 h		4.8×10^3	8.5×10^2	12

The lattice constants are a = 0.88, b = 1.25, and c = 1.336 nm for ε-CL-20, and a = 1.32, b = 0.82, and c = 1.49 nm for γ-CL-20 [15]. By taking into account the percentage change in the CL-20 lattice parameters before and after the phase transition, we can speculate that the major contribution to the thermal expansion is in the a-direction, whereas contraction occurs in the b-direction. The change in the c-direction is relatively small. Therefore, the increases in S_v and ϕ after the phase transition was likely to have been induced by anisotropic thermal expansion. This result is supported by the AFM analysis (Figure 3(b)). An interesting phenomenon was observed, as shown in Figure 4. The strong anisotropic scattering disappeared after the phase transition. We think that the anisotropic scattering was caused by dislocations and/or extended defects (dislocation bundles and small-angle grain boundaries), and can be attributed to two facts. Firstly, dislocations are a commonly observed anisotropic crystal defect in energetic materials [16-18]. The ε-CL-20 crystal is characterized by a large concentration of dislocations (approximately 2×10^7 cm^{-2}) with a Burgers vector of approximately 1 nm [5, 16]. The core size of the dislocations is several or tens of nanometers, which is in the range of the test scale of our SAXS station. Secondly, dislocations in energetic materials, unlike the dislocation loops in metals, are often in the form of straight lines. Therefore, we believe that the strong anisotropic scatterings of the original CL-20 may have originated from the dislocations and/or extended defects of different particles. The reason for the disappearance of the anisotropic scatterings after the phase transition is not very clear, but might be related to the nucleation of a new γ phase or stress cracking at the local sites of the dislocations.

The thermal decomposition reactions, dominated by the homolysis of the $N–NO_2$ bonds of CL-20, involving both unimolecular and bimolecular reactions, can generate gaseous products and elevated pressures within the material [4, 17]. Given sufficient gas production and internal pressurization from the local decomposition reactions, small voids can coalesce into large voids, and macro- and micro-cracks will appear in the samples. Consequently, the complex chemical processes would result in increases in void size, specific surface area, and volume ratio. The microstructure variations of CL-20 caused by thermal treatment are nearly the same as those of HMX. Apparent voids are formed in HMX crystals during thermal decomposition at 235 °C [18]. Peterson *et al*. [8] studied the thermal damage in HMX-based polymer-bonded explosives using SAXS. The microstructure variation in HMX can be classified into two separate temperature regimes: the β–δ phase transition regime (155-174 °C) and the chemical decomposition regime (175-210 °C). The specific surface area of HMX increases by approximately 10 times when the temperature is increased

from 160 to 200 °C, whereas the CL-20 specific surface area increases by two orders of magnitude. Further experiments are necessary in order to investigate the damage mechanisms and to build a correlation between the thermally induced damage and the performance of CL-20.

Conclusions

The microstructural variations of CL-20 caused by thermal treatment have been studied in this work using XRD, AFM, OM, and SAXS. A wave-like process, abrupt volume expansion, movement, and fragmentation of CL-20 particles were observed by in situ variable-temperature OM. After phase transition (160 °C), the CL-20 sample acquired a very rough surface with numerous dimple depressions. S_v and ϕ increased by 5.4 and 5.2-fold, respectively, after the phase transition. A large number of voids were produced both in the bulk and the surface of CL-20 during thermal decomposition. By contrast to the sample heated at 150 °C for 1 h, after heating at 200 °C for 5 h the S_v and ϕ values of the sample increased by factors of about 1.4×10^3 and 2.0×10^3 respectively for large voids with a median size of 120 nm, as well as by factors of about 4.8×10^3 and 8.5×10^2 respectively for small voids with a median size of 12 nm during thermal decomposition.

Acknowledgments

This work was supported by the National Natural Science Foundation of China under grant Nos. 11205137, 11072225 and 11079043.

References

[1] Hsu P.C., De Haven M., McClelland M., Tarver C., Chidester S., Maienschein J.L., Characterization of Damaged Materials, *13th International Detonation Symposium*, Norfolk, Virginia, July 23-28, **2006**, 617.

[2] Willer R.L., The True History of CL-20, *New Trends Res. Energ. Mater.*, *Proc. Semin.*, *16th*, Pardubice, **2013**, 384-394.

[3] Lee J.S., Jaw K.S., Thermal Decomposition Properties and Compatibility of CL-20, NTO with Silicone Rubber, *J. Therm. Anal. Calorim.*, **2006**, *85*, 463-467.

[4] Naik N., Gore G., Gandhe B., Sikder A., Studies on Thermal Decomposition Mechanism of CL-20 by Pyrolysis Gas Chromatography-mass Spectrometry (Py-GC/MS), *J. Hazard. Mater.*, **2008**, *159*, 630-635.

[5] Chukanov N., Dubikhin V., Raevskii A., Golovina N., Korsunskii B., Nedel'ko V., Aldoshin S., Kinetics and Mechanism of a Polymorphous Transition in

Polycrystalline ε-Hexanitrohexaazaisowurtzitane, *Russ. J. Phy. Chem. A*, **2006**, *80*, 281-287.

[6] Teipel U., Particle Processing and Characterization, in: *Energetic Materials*, Weinheim, Wiley-VCH, **2005**.

[7] Mang J.T., Skidmore C.B., Son S.F., Hjelm R.P., Rieker T.P., An Optical Microscopy and Small-Angle Scattering Study of Porosity in Thermally Treated PBX 9501, *AIP Conf. Proc.*, **2002**, *620*, 833-836.

[8] Peterson P.D., Mang J.T., Asay B.W., Quantitative Analysis of Damage in an Octahydro-1,3,5,7-tetranitro-1,3,5,7-tetrazonic-based Composite Explosive Subjected to a Linear Thermal Gradient, *J. Appl. Phy.*, **2005**, *97*, 093507.

[9] Willey T.M., Hoffman D.M., van Buuren T., Lauderbach L., Ilavsky J., Gee R. H., Maiti A., Overturf G., Fried L., In-situ Monitoring of the Microstructure of TATB-based Explosive Formulations During Temperature Cycling Using Ultra-small Angle X-ray Scattering, *Propellants Explos. Pyrotech.*, **2008**, *34*, 406-414.

[10] Huang C.Q., Xia Q.Z., Yan G.Y., Sun G.A., Chen B., A New Package: MySAS for Small Angle Scattering Data Analysis, *Nuc. Sci. Tech.*, **2010**, *21*, 325-329.

[11] Nedelko V., Chukanov N., Raevskii A., Korsounskii B., Larikova T., Kolesova O., Volk F., Comparative Investigation of Thermal Decomposition of Various Modifications of Hexanitrohexaazaisowurtzitane (CL-20), *Propellants Explos. Pyrotech.*, **2000**, *25*, 255-259.

[12] Gump J.C., Stoltz C.A., Peiris S.M., Phase Stability of Epsilon and Gamma HNIW (CL20) at High Pressure and Temperature, *AIP Conf. Proc*., **2007**, *955*, 127-132.

[13] Chen H., Chen S., Li L., Jin S., Quantitative Determination of ε-Phase in Polymorphic HNIW Using X-ray Diffraction Patterns, *Propellants Explos. Pyrotech.*, **2008**, *33*, 467-471.

[14] Mang J.T., Hjelm R.P., Francois E.G., Measurement of Porosity in a Composite High Explosive as a Function of Pressing Conditions by Ultra-Small-Angle Neutron Scattering with Contrast Variation, *Propellants Explos. Pyrotech.*, **2010**, *35*, 7-14.

[15] Sorescu D.C., Rice B.M., Thompson D.L., Molecular Packing and NPT-Molecular Dynamics Investigation of the Transferability of the RDX Intermolecular Potential to 2, 4, 6, 8, 10, 12-Hexanitrohexaazaisowurtzitane, *J. Phy. Chem. B*, **1998**, *102*, 948-952.

[16] Yazici R., Kalyon D., Microstrain and Defect Analysis of CL-20 Crystals by Novel X-Ray Methods, *J. Energ. Mater.*, **2005**, *23*, 43-58.

[17] Geetha M., Nair U., Sarwade D., Gore G., Asthana S., Singh H., Studies on CL-20: the Most Powerful High Energy Material, *J. Therm. Anal. Calorim.*, **2003**, *73*, 913-922.

[18] Behrens R., Thermal Decomposition of HMX: Morphological and Chemical Changes Induced at Slow Decomposition Rates, *12th International Detonation Symposium*, San Diego, California, August 11-16, **2002**.